



Salt-assisted combustion synthesis of cobalt ferrite nanoparticles; magnetic properties and cation distribution measurement by XRD analysis

*Saba Fayazzadeh, Mehdi Khodaei**

Faculty of Materials Science and Engineering, K. N. Toosi University of Technology, Tehran, Iran.

Received: 26 February 2019; Accepted: 23 April 2019

** Corresponding author email: khodaei@kntu.ac.ir*

ABSTRACT

Current study represents the effect of the size and synthesis method on the cation distribution of cobalt ferrite nanoparticles and on the magnetic properties. The nanoferrites have been synthesized through sol-gel auto-combustion method using metal nitrates as precursor and citrate as fuel. In order to obtain the fine and agglomerated-free particles, we have used salt-assisted combustion reaction method. Magnetic properties of the synthesized single phase cobalt ferrite nanoparticles are carried out using vibrating sample magnetometer (VSM) at room temperature. It has been observed that the coercivity and saturation magnetization of the samples reduce by adding salt. The transmission electron microscopy (TEM) confirms the finer nanoparticles formation from around 70-200 nm to 10-40 nm. Structural characterization is done by X-ray diffraction (XRD) and it confirms the spinel structure formation for the samples. The crystallite size and induced strain are derived from the XRD patterns by Williamson-Hall (W-H) method. The magnetic parameters are reduced by crystallite size reduction from 38.5 nm to 11 nm. The further analysis of XRD peaks is fulfilled using Rietveld refinement in order to explain the magnetic properties. The obtained Rietveld refined data allow us to measure the distribution of cations within the available octahedral and tetrahedral sites.

Keywords: *Sol-gel auto-combustion, Magnetic properties, Cobalt ferrite, W-H analysis, Cation distribution, Rietveld refining.*

1. Introduction

Recently, magnetic nanoferrites have attracted researchers' attention in various fields from lithium ion battery [1, 2] to biological applications such as MRI contrast agent [3], drug delivery [4], magnetic fluid hyperthermia [5, 6] and etc. Spinel ferrite nanoparticles can provide extraordinary magnetic, optical and electrical properties [7]. Cobalt ferrite is a hard magnetic material with relatively high coercivity and moderate saturation magnetization. In addition, it has a good chemical and mechanical stability and is a biocompatible material. All these attributes turn it into a reliable candidate for wide

fields of application. Sol-gel auto combustion method is a simple and fast route beside its energy efficiency advantage. Also it provides good chemical homogeneity product with high purity and crystallinity [8]. The major limitation of this method is a difficulty of preventing agglomeration. Addition of inert salt such as NaCl and KCl to the conventional sol-gel auto-combustion route can compensate this deficiency. During the solution combustion process, solvent evaporation as a results of high temperature combustion causes the formation of salt crust thin layer on the surface of the forming nanoparticles. After the reaction and

cooling, the frozen salt matrix acts as a barrier and inhibits re-agglomeration of particles. The trapped nanoparticles can be easily washed and dried in order to get rid of crusted salts on their surface [9, 10]. Hence, salt-assisted auto-combustion method can be used as a facile and low cost method for preparing separated nanoparticles.

The physical properties of spinel ferrites strongly depend on stoichiometry, preparation procedure and the distribution of cations among the interstitial sublattice sites [11]. Spinel ferrite with general molecular formula of $(M^{2+})[Fe_2^{3+}]O_4^{2-}$ containing divalent (M^{2+} ; $M = Mn, Fe, Co, Ni$ and Zn) and trivalent (Fe^{3+}) cations. A unit cell of a spinel ferrite containing eight formula units that form face-centered cubic (FCC) structure belonging to $Fd\bar{3}m$ special group [12]. There are 64 tetrahedral (A sites) and 32 octahedral (B sites) possible interstitial sites for placing cations in the unit cell. Divalent cations occupy 8 sites of tetrahedral (a-Wyckoff position) and trivalent cations occupy the 16 octahedral (d-Wyckoff position) sublattice and 32 oxygen atoms in close cubic packing (e-Wyckoff position) [13]. Each A- and B-site is surrounded by 4 and 6 O^{2-} ions, respectively. So, the O^{2-} ions have a four-fold coordination formed by three B cations and one A cation [11]. Spinel have asymmetric unit constituted by two cations on special positions and one oxygen atom that has symmetry coordinates in order to be (u,u,u) [13]. It should be noted that the detailed position of oxygen ions at FCC sublattice is described by u parameter because the O^{2-} ions are not placed at exact position of the FCC sublattice. The u parameter reflects adjustments of the structure to accommodate differences in the radius ration of the cations in the A and B sites. This parameter can have the value of 0.375 or 0.25 due to its center of symmetry. However, most of the known spinels have higher value than 0.375 because the ideal structure almost never can be obtained [11]. The general formula of a spinel ferrite is $(M^{2+}_{1-x} Fe^{3+}_x)[M_x Fe^{3+}_{2-x}]O_4$ that clearly represents the distribution of cations through tetrahedral and octahedral sites and x shows the degree of inversion which corresponds to the M cation occupation on octahedral site [13]. This value varies from zero to one, where the normal and the inverse structure have value of zero and one, respectively, and every other fraction represents the mixed spinel structure [14]. Ionic radius, crystal field, electronic configuration and ionic polarization are determinative factors in the

cation site occupation [11]. Determination of the cations distribution on tetrahedral and octahedral sites is necessary to understand the magnetic properties [15]. Although there are many technics exploited based on XRD in order to study the cation distribution of spinel ferrites, all of them are based on the observed experimentally and calculated XRD peak intensities comparison [11].

As mentioned before, the synthesis method is an effective factor for the cation distribution and consequently the magnetic properties [14]. The synthesis method not only can change the particle size but also can induce strain in nanoparticles and this intrinsic induced micro-strain change the cation distribution among octahedral and tetrahedral sites [16].

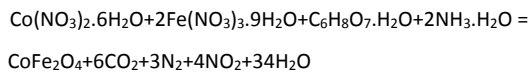
In this paper, the $CoFe_2O_4$ nanoparticles have been synthesized through conventional and salt-assisted sol-gel auto combustion method in order to observe the effect of synthesis method on the magnetic properties. The cation distribution in spinel structure of $CoFe_2O_4$ nanoparticles synthesized by different combustion methods has been obtained by XRD analysis and its dependence on the magnetic properties of $CoFe_2O_4$ is investigated in details.

2. Materials and methods

Cobalt nitrate ($Co(NO_3)_2 \cdot 6H_2O$) and iron nitrate ($Fe(NO_3)_3 \cdot 9H_2O$) were used as cation sources, citric acid ($C_6H_8O_7$) was selected not only as fuel but also as chelating agent. In this work, the pH was adjusted by ammonia (NH_4OH), and potassium chloride (KCl) was applied in the salt-assisted method. All the reagents provided from Merck Co. and used as received without any purification.

Simple sol-gel auto combustion was applied for synthesis of cobalt ferrite nanoparticles. Adequate amount of nitrates was mixed together in deionized water in order to have an aqueous solution with 1:2 molar ratio of Co and Fe cations. Citric acid was added to the solution in equal molar ratio of whole cations to ensure the reaction took place completely [17]. It was kept stirring until all the reagents dissolved and resulting in a clear orange solution. Then, ammonia solution was added drop wise in order to controlling the pH of the solution. The pH was adjusted at around 7 based on the pervious works [8]. Subsequently, the solution was heated to $100^\circ C$ and kept stirring to evaporation of excess water. In this stage, a viscous brown gel was formed and the combustion reaction was going

to start by raising the temperature. The following self-propagation reaction led to form of black ash. The synthesized cobalt ferrite nanoparticles by conventional combustion method named as “sample I” from now on. The obtained powder was ready for characterization without any further heat treatment. The chemical reaction can be expressed as:



This reaction is a self-propagating exothermic oxidant-reduction reaction in which metal nitrates are oxidant and citric acid is reducing agent. The carboxyl groups of citric acid have two simultaneous roles; act as a fuel and also as a chelating agent to produce both necessary heat of the reaction as well as chelation the cations for producing the stoichiometry CoFe_2O_4 compound without any impurities.

The salt-assisted synthesis is similar to the mentioned procedure except as the salt (KCl) was added to the solution after adjusting the pH with 2:3 molar ratio of salt to oxidizer. This salt is solved in aqueous media and during the combustion (evaporation of aqueous solvent), it will be crusted on the synthesized nanoparticles. After synthesis, the grinded powder was washed three times using deionized water in order to remove the salt and dried in oven at 120°C for 24 hours. The nanoparticles prepared by this method known as “sample II” in the following context.

The shape and particle size of the synthesized cobalt ferrite nanoparticles observed by transmission electron microscopy (TEM) performed by JEOL, JEM-2100F microscope operating at 200 kV. Sample preparation process after combustion for TEM analysis was included the washing and drying and subsequent dispersion in ethanol, which was same for both samples. The powder X-ray diffractometry (XRD) was done for phase identification and structural analysis, crystallite size and mean lattice strain calculation. XRD Philips X’Pert Pro diffractometer was used with Cu $\text{K}\alpha$ radiation of wavelength 0.154056 nm in 2θ range of 20°-80°. In the first step, the phase identification was done by X’Pert High Score Plus software and additional analysis (cation distribution measurement) was performed by MAUD software. The magnetic properties were measured by a vibrating sample magnetometer (VSM) (Meghnatis Daghigh Kavir Co., Iran) with a maximum applied field of 9 kOe.

3. Results and discussion

As aforementioned, salt-assisted auto-combustion method can be used as a facile and low cost method for preparing oxide ceramics nanoparticles with smaller particle size in comparison to the conventional auto-combustion method. In order to find out the effect of synthesis method on the size and shape of CoFe_2O_4 nanoparticles, the TEM analysis has been performed. It is worth to notice that both samples had a similar preparation process after combustion for TEM analysis (washing and drying and

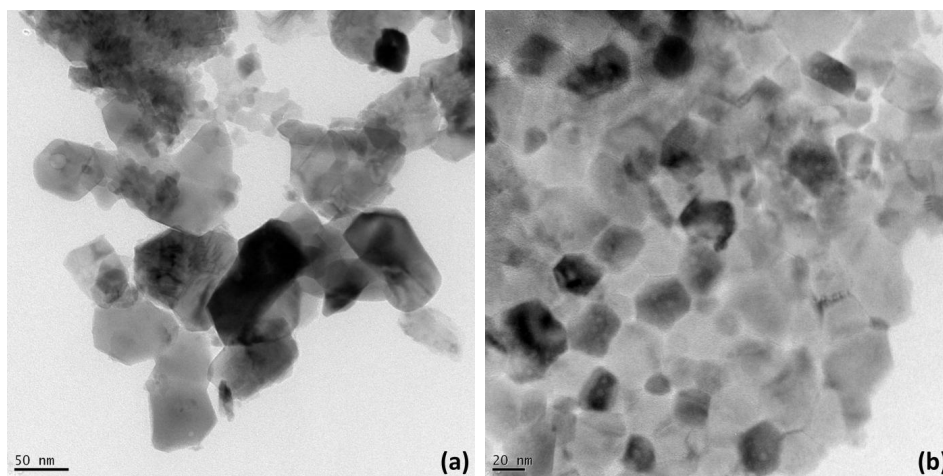


Fig. 1- TEM images of prepared cobalt ferrite nanoparticles; (a) synthesized by conventional combustion (sample I), (b) synthesized by salt-assisted combustion (sample II).

subsequent dispersion in ethanol) as mentioned in the experimental section. TEM images of the synthesized cobalt ferrite nanoparticles (Fig. 1), show that the particle size of sample I is around 70 to 200 nm which confirms the wide size distribution of these irregular shape nanoparticles (Fig. 1(a)). However, as can be seen in Fig. 1(b), sample II has a polygonal shape particles and the particles sizes vary from 10 to 40 nm. This finer size clarifies that the salt acts as a nano-scale reactor [10], which can control the growth of newly formed nanoparticles by formation of a crust after aqueous solution evaporation during combustion [9, 10]. The TEM images of the prepared samples clearly reveal the effect of addition of salt to the solution on the size and distribution of the particles. It can be concluded that finer particles are formed due to the limitation of particle growth by KCl crust formation during combustion. Although, it has been demonstrated that the final size is exclusively determined by the nucleation and growth kinetics at early times of

chemical reaction [18-20], the presence of salt in the solution that can be crusted on the surface of nanoparticles can stop the growth step.

XRD patterns of both samples prepared by conventional and salt-assisted sol-gel auto-combustion methods are shown in Fig. 2. The obtained peaks confirm the single phase cobalt ferrite formation according to the good agreement with ICDD PDF card No. 22-1086. The realized peak indices; (111), (220), (311), (400), (422), (511) and (440) correspond to the cubic spinel structure with space group $Fd\bar{3}m$. We can assure that the cobalt ferrite phase is formed completely because there is not any extra peak in the both XRD patterns corresponds to impurity, especially Fe_2O_3 . The good crystallinity and single phase formation can be related to the appropriate selection of fuel to metal nitrate ratio and pH. As it is obvious from Fig. 2, addition of salt leads to XRD peak broadening. There are several parameters that effect on broadening of the XRD peaks. Crystallite size is one of the important properties extracted from the peak width. The well-known Scherrer formula estimate the crystallite size of nanoparticles from the XRD patterns using the equation 1;

$$t = k\lambda/\beta\cos\theta \quad (\text{eq. 1})$$

where k is the shape factor equal to 0.9 for the spherical particles assumption. λ is the radiation of wavelength (1.54 Å). β and θ are full width at half maximum of the intensity and Bragg's diffraction angle, respectively. The average crystallite sizes of the synthesized nanoparticles (calculated based on 3 different peaks) are listed in Table 1. It indicates that the crystallite size reduced by applying salt to the conventional sol-gel auto combustion method. The possible size reduction mechanism will be discussed below. Since using the Scherrer formula is a common way to measure the crystallite size in most of the studies, it has to be considered that this method just provides the lower limit of the crystallite size [21]. In addition, the peaks

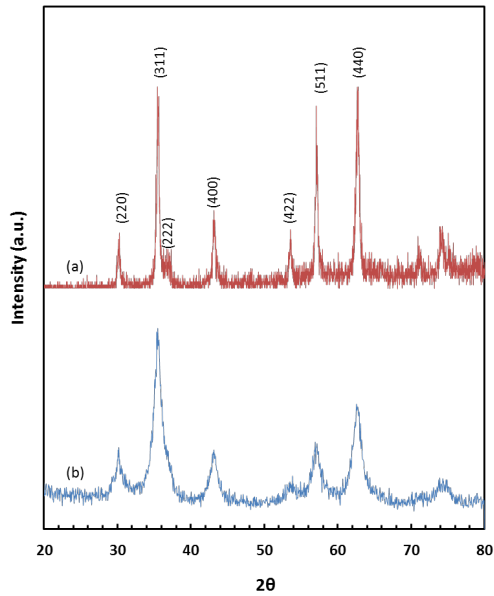


Fig. 2- XRD patterns of synthesized cobalt ferrite nanoparticles; a) synthesized by conventional combustion (sample I), (b) synthesized by salt-assisted combustion (sample II).

Table 1- The crystallite size and strain of the samples synthesized by conventional combustion (sample I) and synthesized by salt-assisted combustion (sample II)

	Average Crystallite size (nm) Scherrer	W-H	Average Mean Lattice Strain ($\times 10^{-3}$)
Sample I	16.6±2.1	38.50	2.90
Sample II	5.3±0.4	11.00	8.37

broadening of nanomaterials can be affected not only by crystallite size but also by lattice strain. Therefore, in order to obtain the precise crystallite size, induced lattice strain calculations should be taken in to account [22]. The Williamson-Hall (W-H) method is used for determining average lattice strain and grain size because of its ability to deconvolute the size-induced and strain-induced broadening contribution by considering the peak width [23]. The equation 2 presents the W-H equation in which ϵ is the microstrain induced in the lattice:

$$\beta = k\lambda/t\cos\theta + 4\epsilon\sin\theta \quad (\text{eq. 2})$$

The W-H method assumes this strain is presented uniformly in every direction of crystallographic lattice [21]. We can estimate the average crystallite size and microstrain by plotting and extrapolating the $\beta\cos\theta$ versus $\sin\theta$ values (Fig. 3). The grain size and induced strain are extracted from the slope and the Y-intercept, respectively. The calculated crystallite size and induced microstrain through the W-H method are tabulated in Table 1. It is observed that the size reduction with salt addition in the conventional synthesis method is confirmed by this method too and it is reasonable with the obtained TEM particles sizes. Since the self-propagating reaction releases large amount of heat in a short time and the temperature of the reaction system goes up instantly, a thin layer salt crust is formed on the newly formed nanoparticle surface in order to diminish the free energy of system.

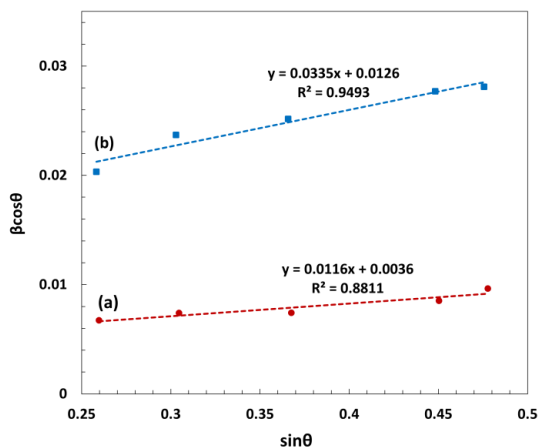


Fig. 3- Williamson-Hall (W-H) plot of synthesized cobalt ferrite nanoparticles; a) synthesized by conventional combustion (sample I), (b) synthesized by salt-assisted combustion (sample II).

After cooling, the salt-coated nanoparticles trap in the frozen salt matrix and cannot move anymore. Thus, the finer particles are synthesized through salt-assisted method and they are prevented from re-agglomeration [10]. The estimated microstrain of the sample I is 2.9×10^{-3} whereas for the sample II this value is 8.37×10^{-3} . This induced-strain enhancement can be related to the reaction condition that discussed above.

In order to investigate the effect of size reduction on the magnetic properties as a result of addition of salt to the conventional sol-gel auto-combustion synthesis, the VSM test was done at room temperature. The coercivity and saturation magnetization of the prepared samples extracted from the M-H hysteresis loops are listed in Table 2. It indicates that the coercivity is reduced from 1266 Oe to 328 Oe by the particle size reduction of the synthesized samples. Such relatively high coercivity value for the conventional synthesized sample is attributed to the large size of the particles and can be assumed that they are in the multi-domain region based on Chennasamy et al. [24]. They have reported that the critical single domain size for the cobalt ferrite nanoparticles is 40 nm and found a coercivity value as high as 4.65 kOe for such particles [24]. Hence, the coercivity reduction of our samples can be completely justifiable by size effect on the coercivity values graph represented in Fig. 4. It shows that the coercivity value increases proportional to $1/D$ (where D is the particle size) until reaches to its maximum value at the critical single domain size and then reduces. It should be noted that the measured magnetic properties by VSM are the average data related to the whole of samples. Hence, the data are shown in Fig. 4 for an average particle size of samples. Thus, it can be concluded that small nanoparticles synthesized through salt-assisted sol-gel auto-combustion method are in single domain region and their coercivity is lower as a results of single domain state.

In addition, saturation magnetization also reduced with decreasing the nanoparticle size. From one aspect, this reduction from 54 emu/g to 31.3 emu/g can be attributed to the effect of particle size on the formation of magnetic dead layer and thus on the saturation magnetization. The magnetic spins on the surface of nanoparticles do not have a certain direction and may become canted. These canted spins on the particles

surface form a magnetically dead layer and lead to reduce the total number of oriented spins and consequently lead to the decrease in the saturation magnetization. As it is shown in Fig. 5, the dead layer on the nanoparticle surface containing canted spins become more considerable for the smaller particles due to its constant thickness [25]. It is worth to mention that the magnetic surface anisotropy can be also the reason for altering the magnetic properties of cobalt ferrite nanoparticles by decreasing the particle size [15].

On the other hand, the reduction of saturation magnetization is related to the cation distribution through the octahedral and tetrahedral sites. In order to obtain the cation distribution Rietveld analysis of XRD peaks was done by MAUD software, which is the main subject of the present work.

The refined XRD graphs are shown in Fig. 6. The distribution of cations in both octahedral and tetrahedral sites is listed in Table 2. The magnetic moment per formula unit ($\mu_{\psi\upsilon}$) of a spinel ferrite

can be calculated theoretically using Neel's two-sublattice model by considering the difference of total magnetic moments in octahedral and tetrahedral sites;

$$\mu = M_{\text{tetrahedral}} - M_{\text{octahedral}} \quad (\text{eq. 3})$$

The net magnetic moment $\mu_{\psi\upsilon}(\beta)$ of Co^{2+} and Fe^{3+} is $3 \mu_B$ and $5 \mu_B$, respectively. The calculated values for both samples are listed in Table 2 and reveals that the magnetic moment reduces from $5.32 \mu_B$ to $3.48 \mu_B$ by the variation of cation distribution. In conclusion, it can be said that increasing the degree of inversion lead to saturation magnetization reduction.

This value also can be measured experimentally by the following equation in Bohr magneton;

$$\mu_B = \text{Mol.wt} \times M_s / 5585 \quad (\text{eq. 4})$$

The calculated values tabulated in Table 2, confirm the magnetic moment reduction through experimental calculation too. It can be considered

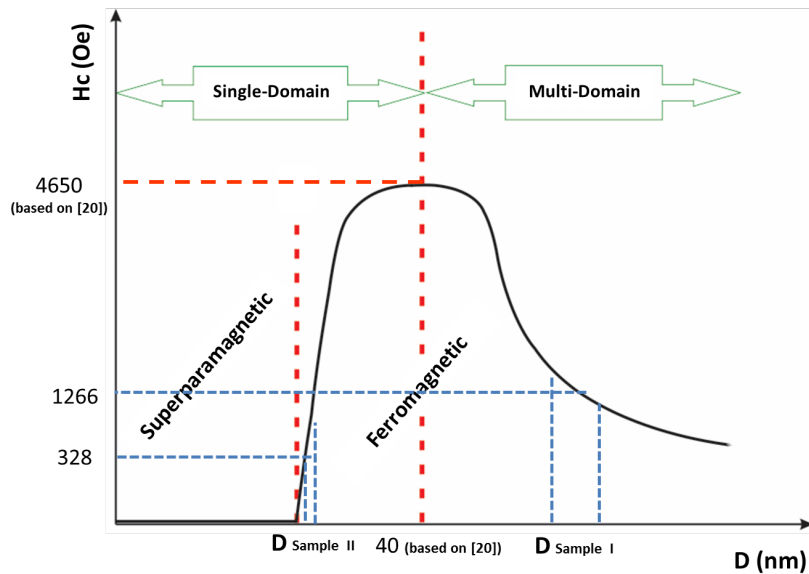


Fig. 4- Relationship of the particle size and the coercivity from multi domain to single domain region, representing the coercivity of critical single domain size in CoFe_2O_4 [20] as well as CoFe_2O_4 nanoparticles synthesized by conventional combustion (sample I) and synthesized by salt-assisted combustion (sample II).

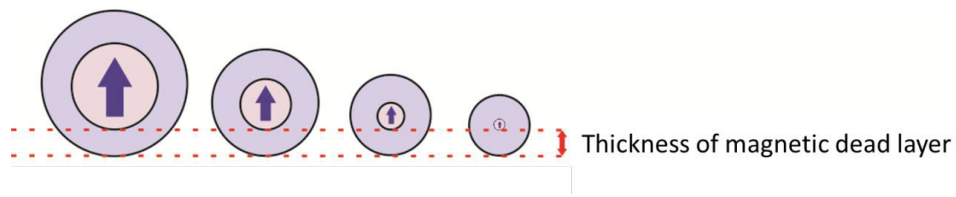


Fig. 5- Schematic presentation of the effect of particle size on the magnetic dead layer.

that the magnetic ions on A and B sites are coupled ferromagnetically within each sublattice and antiferromagnetically between sublattices [11].

However, the calculated data from XRD and VSM are not coincident, which can be related to the finite size of nanoparticles leading to the non-

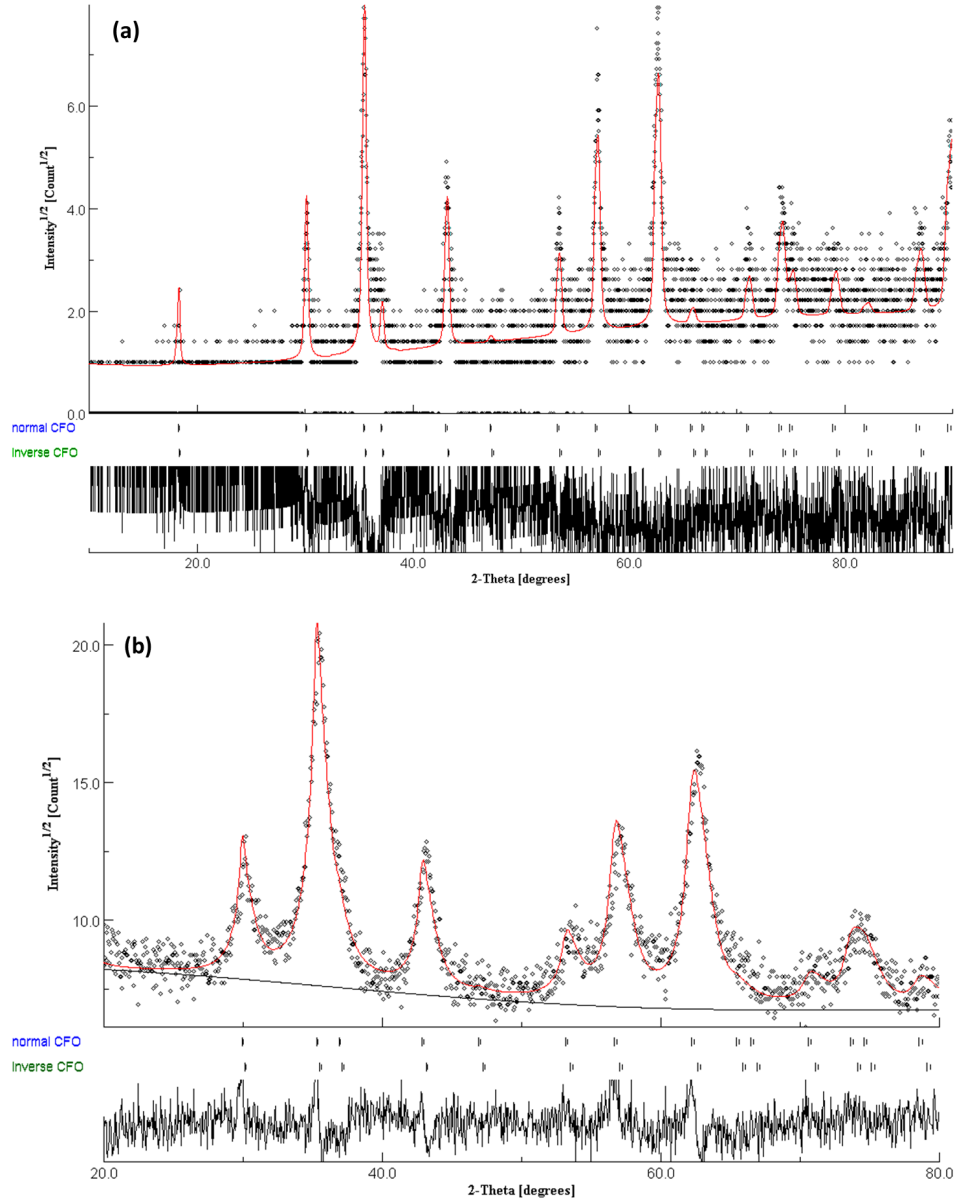


Fig. 6- Refinement plots of the samples (a) sample I and (b) sample II using MAUD software.

Table 2- cation distribution and magnetic properties of prepared samples

	Hc (Oe)	Ms (emu/g)	μ_B (exp)	Cation distribution	μ_B (theory)
Sample I	1266	54	2.27	(Co _{0.58} Fe _{0.42})[Co _{0.42} Fe _{1.58}]O ₄	5.32
Sample II	328	31.3	1.32	(Co _{0.12} Fe _{0.88})[Co _{0.88} Fe _{1.12}]O ₄	3.48

collinearity of magnetic moments on the surface of the nanoparticles. The disordered moments are formed due to the broken exchange bonds at the outer layer. On the other hand, the competition of antiferromagnetic interactions leads to a non-collinear arrangement of magnetic moments within interstitial sublattices which is induced because of the non-equilibrium cation distribution among tetrahedral and octahedral sites.

4. Conclusion

Single phase cobalt ferrite nanoparticles have been synthesized using a citrate-nitrate sol-gel auto-combustion method. The crystallite size of the sample synthesized by conventional auto-combustion is 38.5 nm whereas by introducing salt to the conventional method it reduces to 11 nm. The Williamson-Hall equation shows that salt addition induced more strain in the lattice structure of the spinel ferrite. The magnetic measurement has shown that both coercivity and saturation magnetization decreased by particle size reduction. The coercivity reduction can be explained by the relationship between the coercivity and particle size. The saturation magnetization of CoFe_2O_4 nanoparticle synthesized by conventional and salt-assisted combustion is 54 emu/g and 31.3 emu/g, respectively, which can be related to the more canted spins on the surface of finer particles due to the surface effect of nanoparticles. Furthermore, it is affected by the cation distribution through the possible sublattice sites. In order to obtain the distribution of cations within octahedral and tetrahedral sites, the Rietveld analysis of the XRD patterns was done. Hence, the magnetic properties are validated using the results of cation distribution.

References

1. Wang G, Wang H, Bai J. Preparation and electrochemical evaluation of manganese ferrite spheres as anode materials for half and full lithium-ion batteries. *Journal of Alloys and Compounds*. 2015;627:174-81.
2. Sun X, Zhu X, Yang X, Sun J, Xia Y, Yang D. CoFe_2O_4 /carbon nanotube aerogels as high performance anodes for lithium ion batteries. *Green Energy & Environment*. 2017;2(2):160-7.
3. Hankiewicz JH, Stoll JA, Stroud J, Davidson J, Livesey KL, Tvrđy K, et al. Nano-sized ferrite particles for magnetic resonance imaging thermometry. *Journal of Magnetism and Magnetic Materials*. 2019;469:550-7.
4. Zamani M, Naderi E, Aghajanzadeh M, Naseri M, Sharafi A, Danafar H. $\text{Co}_1\text{-XZn}_x\text{Fe}_2\text{O}_4$ based nanocarriers for dual-targeted anticancer drug delivery: Synthesis, characterization and in vivo and in vitro biocompatibility study. *Journal of Molecular Liquids*. 2019;274:60-7.
5. Vamvakidis K, Mourdikoudis S, Makridis A, Paulidou E, Angelakeris M, Dendrinou-Samara C. Magnetic hyperthermia efficiency and MRI contrast sensitivity of colloidal soft/hard ferrite nanoclusters. *Journal of Colloid and Interface Science*. 2018;511:101-9.
6. Shahjuee T, Masoudpanah SM, Mirkazemi SM. Coprecipitation Synthesis of CoFe_2O_4 Nanoparticles for Hyperthermia. *Journal of Ultrafine Grained and Nanostructured Materials*. 2017 Dec 1;50(2):105-10.
7. Shanmugavel T, Raj SG, Rajarajan G, Kumar GR, Boopathi G. Single Step Synthesis and Characterisation of Nanocrystalline Cobalt Ferrite by Auto-Combustion Method. *Materials Today: Proceedings*. 2015;2(4-5):3605-9.
8. Sutka A, Mezinskis G. Sol-gel auto-combustion synthesis of spinel-type ferrite nanomaterials. *Frontiers of Materials Science*. 2012;6(2):128-41.
9. Zhang X, Jiang W, Song D, Sun H, Sun Z, Li F. Salt-assisted combustion synthesis of highly dispersed superparamagnetic CoFe_2O_4 nanoparticles. *Journal of Alloys and Compounds*. 2009;475(1-2):L34-L7.
10. Chen W, Li F, Yu J. Salt-assisted combustion synthesis of highly dispersed perovskite NdCoO_3 nanoparticles. *Materials Letters*. 2007;61(2):397-400.
11. Najmoddin N, Beitollahi A, Kavas H, Majid Mohseni S, Rezaie H, Åkerman J, et al. XRD cation distribution and magnetic properties of mesoporous Zn-substituted CuFe_2O_4 . *Ceramics International*. 2014;40(2):3619-25.
12. Kumar L, Kumar P, Narayan A, Kar M. Rietveld analysis of XRD patterns of different sizes of nanocrystalline cobalt ferrite. *International Nano Letters*. 2013;3(1).
13. Levy D, Pavese A, Hanfland M. Phase transition of synthetic zinc ferrite spinel (ZnFe_2O_4) at high pressure, from synchrotron X-ray powder diffraction. *Physics and Chemistry of Minerals*. 2000;27(9):638-44.
14. Pourgolmohammad B, Masoudpanah SM, Aboutalebi MR. Synthesis of CoFe_2O_4 powders with high surface area by solution combustion method: Effect of fuel content and cobalt precursor. *Ceramics International*. 2017;43(4):3797-803.
15. Peddis D, Yaacoub N, Ferretti M, Martinelli A, Piccaluga G, Musinu A, et al. Cationic distribution and spin canting in CoFe_2O_4 nanoparticles. *Journal of Physics: Condensed Matter*. 2011;23(42):426004.
16. Singh S, Khare N. Defects/strain influenced magnetic properties and inverse of surface spin canting effect in single domain CoFe_2O_4 nanoparticles. *Applied Surface Science*. 2016;364:783-8.
17. Pubby K, Meena SS, Yusuf SM, Bindra Narang S. Cobalt substituted nickel ferrites via Pechini's sol-gel citrate route: X-band electromagnetic characterization. *Journal of Magnetism and Magnetic Materials*. 2018;466:430-45.
18. Mozaffari S, Li W, Thompson C, Ivanov S, Seifert S, Lee B, et al. Colloidal nanoparticle size control: experimental and kinetic modeling investigation of the ligand-metal binding role in controlling the nucleation and growth kinetics. *Nanoscale*. 2017;9(36):13772-85.
19. Li W, Ivanov S, Mozaffari S, Shanaiah N, Karim AM. Palladium Acetate Trimer: Understanding Its Ligand-Induced Dissociation Thermochemistry Using Isothermal Titration Calorimetry, X-ray Absorption Fine Structure, and ^31P Nuclear Magnetic Resonance. *Organometallics*. 2018;38(2):451-60.
20. Mozaffari S, Li W, Thompson C, Ivanov S, Seifert S, Lee B, et al. Ligand-Mediated Nucleation and Growth of Palladium Metal Nanoparticles. *Journal of Visualized Experiments*. 2018(136).
21. Irfan H, Racik K M, Anand S. Microstructural evaluation of CoAl_2O_4 nanoparticles by Williamson-Hall and size-strain plot methods. *Journal of Asian Ceramic Societies*. 2018;6(1):54-62.
22. Jamil MT, Ahmad J, Bukhari SH, Saleem M. Effect of Re and Tm-site on morphology structure and optical band gap of ReTmO_3 (Re: La, Ce, Nd, Gd, Dy, Y and Tm: Fe, Cr) prepared by sol-gel method. *Revista Mexicana de Física*. 2018;64(4):381.
23. Augustin M, Balu T. Estimation of Lattice Stress and Strain in Zinc and Manganese Ferrite Nanoparticles by Williamson-Hall and Size-Strain Plot Methods. *International Journal of Nanoscience*. 2017;16(03):1650035.

24. Chinnasamy CN, Jeyadevan B, Shinoda K, Tohji K, Djayaprawira DJ, Takahashi M, et al. Unusually high coercivity and critical single-domain size of nearly monodispersed CoFe₂O₄ nanoparticles. *Applied Physics Letters*. 2003;83(14):2862-4.
25. Shin T-H, Choi Y, Kim S, Cheon J. Recent advances in magnetic nanoparticle-based multi-modal imaging. *Chemical Society Reviews*. 2015;44(14):4501-16.